

## Original papers

# Development of a high-throughput plant disease symptom severity assessment tool using machine learning image analysis and integrated geolocation



James W. Clohessy <sup>a,\*</sup>, Santosh Sanjel <sup>a,b</sup>, G. Kelly O'Brien <sup>a</sup>, Rebecca Barocco <sup>a,b</sup>, Shivendra Kumar <sup>a,b</sup>, Scott Adkins <sup>d</sup>, Barry Tillman <sup>a,c</sup>, David L. Wright <sup>a,c</sup>, Ian M. Small <sup>a,b,\*</sup>

<sup>a</sup> North Florida Research and Education Center, University of Florida, Quincy, FL 32351, United States

<sup>b</sup> Department of Plant Pathology, University of Florida, Gainesville, FL 32611, United States

<sup>c</sup> Department of Agronomy, University of Florida, Gainesville, FL 32611, United States

<sup>d</sup> United States Department of Agriculture, Agricultural Research Service, US Horticultural Research Laboratory, United States Department of Agriculture, Fort Pierce, FL 34945, United States

## ARTICLE INFO

### Keywords:

High-throughput  
Phenotyping  
Plant disease  
Machine learning  
Computer vision

## ABSTRACT

Tomato spotted wilt virus (TSWV) has the potential to cause severe yield losses in peanut (*Arachis hypogaea* L.), an important annual legume grown around the world. The most effective approach to manage the disease caused by TSWV is to grow disease resistant peanut varieties. One of the key challenges to breeding for disease resistance is to develop an accurate, reproducible and efficient disease assessment method. Accurate field-based assessment of disease incidence and severity is technically challenging and time-consuming. To address this challenge, a field-based, high-throughput assessment tool was developed to quantify the spatial distribution of disease symptoms over experimental peanut plots using a Real Time Kinematic Global Positioning System (RTK-GPS), consumer-grade cameras, a microcontroller, and an open-source machine learning software. A field experiment was designed to establish a range of disease incidence and severity scenarios. This field experiment was imaged for two seasons to develop and validate the tool. Using transfer learning, an existing Convolutional Neural Network (CNN) was trained from supervised training imagery to classify and quantify areas within the plot-level imagery as, symptomatic, asymptomatic, or ground. Multiple images were assessed by the machine learning model and georeferenced to individual experimental plots using RTK-GPS data. The CNN model trained to detect the symptom, "stunting and mottling", was evaluated using Receiver Operating Characteristic (ROC) curve analysis and yielded an Area Under the Curve (AUC) of 0.97, sensitivity of 0.77, and specificity of 0.98 on the test set. Results from the disease assessment tool were compared with results from visual disease assessments, conducted by a trained plant pathologist. Field plot level means from CNN-based assessment of stunting and mottling correlated with plot level means from visual assessment of severity ( $r = 0.78$ ;  $P < 0.0001$ ). To further validate the CNN-based method, the TSWV field experiment was analyzed using linear mixed models with both visual severity and CNN-based severity assessments used as responses. Both models (visual or CNN-based assessment) identified the same main effects as being significant and post hoc analysis resulted in the same separation of varieties for their severity of TSWV symptoms. The results of this study demonstrate the successful application of this tool for high-throughput disease severity assessment in peanut under field conditions.

## 1. Introduction

Plant disease epidemics severely affects the quality and yield of agricultural produce, and ultimately threaten food security (Strange and Scott, 2005; Madden et al., 2017; Savary et al., 2019). Quantification of

disease is fundamental to (a) determine crop losses; (b) conduct disease surveys; (c) establish thresholds for decision-making; (d) improve knowledge of disease epidemiology, and (e) evaluate the effect of treatments (e.g. variety, fungicides, etc.) (Bock et al., 2020). Plant diseases are typically quantified in terms of incidence or severity at the

\* Corresponding authors at: North Florida Research and Education Center, University of Florida, Quincy, FL 32351, United States.

E-mail addresses: [jameswclohessy@gmail.com](mailto:jameswclohessy@gmail.com) (J.W. Clohessy), [ismall@ufl.edu](mailto:ismall@ufl.edu) (I.M. Small).

field/plot scale and below. For our purposes we define disease incidence as the proportion of the plant units that are diseased in a defined population or sample and disease severity as the proportion of the plant unit exhibiting visible disease symptoms (Madden et al., 2017). Traditionally, disease incidence and severity assessment has relied upon visual estimation. Bock et al. (2020) defines visual estimation as “the action of assigning a value to severity of symptoms perceived by the human eye.” Unfortunately, significant inter- and intra-rater variability can occur, which can impact accuracy and reproducibility of the analysis (Bock et al., 2020).

Advances in optical sensor and image analysis technology provide an alternative means to quantify disease through remote sensing (Nilsson, 1995). These technologies are already being used to detect and quantify disease symptoms, particularly within plant breeding to assist with phenotyping of disease severity (Mahlein, 2016). Application of these methods within highly variable field settings is an area requiring further research (Bock et al., 2020). To address this challenge, we have developed a remote sensing platform and image analysis method to quantify disease severity under field conditions and applied it to quantify symptoms of an important disease of peanut (*Arachis hypogaea* L.).

Cultivated peanut is an important annual legume grown in the semi-arid tropics and subtropics around the world (Naidu et al., 1999). In the United States, the total acreage of peanuts was reported to be 1.4 million acres in 2018 accounting for over 2.4 million metric tons of peanut production, adding over 1 billion dollars to the economy (FAO, 2020). One of the major diseases impacting peanut production in the US is caused by tomato spotted wilt virus (TSWV; species *Tomato spotted wilt orthotospovirus*; genus *Orthotospovirus*; family *Tospoviridae*). Management of TSWV in peanut production typically involves an integrated approach, with variety resistance and application of in-furrow insecticide as two key components (Anco et al., 2019). Resistance against TSWV remains a top priority in peanut breeding programs. However, there are currently no TSWV tolerant peanut varieties available. Some moderately resistant varieties have been released, but they suffer yield losses under conditions of high disease pressure (Culbreath and Srinivasan, 2011). Evaluation and screening of peanut varieties for their resistance to TSWV is a key step before the release of a new TSWV resistant/tolerant peanut varieties which is a time-consuming process (Culbreath et al., 2003). A high-throughput method to assess varieties accurately and reproducibly for TSWV symptoms across environments will improve selection efficiency and accelerate the release of resistant peanut varieties.

Technological advancements in image analysis and machine learning methods have provided new opportunities for crop symptom detection and quantification. Neural networks have been developed as a successful tool for pattern recognition and are a set of interconnected nodes that can be trained via machine learning methods to identify patterns within data (Albawi et al., 2017; Rumelhart, 1986). A Convolutional Neural Network (CNN) is a type of artificial neural network structure that works best for image pattern identification by assembling the interconnected layers in a hierarchical structure of other smaller patterns (Krizhevsky et al., 2012). Various CNN models have been developed in the past for numerous agricultural needs, including plant disease symptoms in a wide variety of crops (DeChant et al., 2017; Fuentes et al., 2017; Kc et al., 2019; Liu et al., 2018; Mohanty et al., 2016; Ma et al., 2018; Ramcharan et al., 2017; Sladojevic et al., 2016; Zhang et al., 2018), though none of these examples provided a high-throughput and ground-based system that could be used under field conditions. Mobile platforms that measure disease severity by visual imagery are less common and have been identified as a research priority (Bock et al., 2020).

Utilizing automated methods and imagery requires the accurate geolocation of sensor data to the appropriate experimental plot. Conventional global positioning systems provide horizontal accuracies of approximately 1.5–2.5 m (Deckert and Bolstad, 1996; Lee et al., 2016), which is insufficient for the typical spacing of experimental plots. A

Real-Time Kinematic Global Positioning System (RTK-GPS) improves this by including a ground reference station that provides wireless real-time corrections to each position. RTK-GPS can be a high-cost component in the system, but low-cost alternatives have recently emerged in the market with sufficient horizontal accuracies of 5 cm or less (Jackson et al., 2018).

Our objective for this study was to develop a field-based high-throughput disease symptom phenotyping system as a proof of concept to enhance field crop disease phenotyping studies. We hypothesize that image analysis tools can be used to effectively and efficiently assess TSWV symptom severity. To examine the effectiveness and efficiency of the system, we tested the resulting CNN model performance against similar images and compared the final phenotyping system results to a conventional visual estimation method used to assess peanut TSWV field experiments.

## 2. Materials and methods

### 2.1. Image and geographic data collection system

The imaging system was comprised of two consumer-grade 24.3 mega-pixel mirrorless Sony a6000 cameras (Sony Corporation, Minato City, Japan), with 16–50 mm f/3.5–5.6 lenses. The cameras were configured to collect raw images, the lens focal length was set to 16 mm, the shutter priority was fixed at 1/1000 s, and all other settings were set to automatic. Left and right cameras were positioned horizontally across the front hydraulic boom of an Avenger tractor (LeeAgra, Lubbock, TX, USA) using a custom 90° bracket, setting the cameras in a nadir position to the crop canopy. A nylon light diffusion fabric (Shenzhen Neewer Technology Co., Ltd, Guangdong, China), typically used for photography light diffusion panels, was attached to a custom built frame structure on the hydraulic boom to provide diffuse lighting over the area being photographed.

The positioning system used a low-cost Piksi Multi RTK-GPS Evaluation Kit (Swift Navigation, San Francisco, CA, USA), which comprised of the RTK-GPS processor, input/output development board, wireless communications board, and antennas for both the base station and rover. The rover RTK-GPS was interfaced with a Raspberry Pi 3 micro-computer (Raspberry Pi Foundation, Cambridge, UK) via a serial to USB connection, and a Python script was used to write RTK-GPS outputs to a microSD card. The Python script output provided a CSV format file with WGS84 RTK-GPS corrected coordinates and GPS satellite timestamps at an interval of ten times per second. The Raspberry Pi triggered the a6000 cameras at the frequency of once per second by delivering + 5 V to the camera trigger and focus wires within the Sony Multiport interface on both a6000 cameras simultaneously.

The RTK-GPS base station was temporarily installed outside the field of interest, within line-of-site of the wireless antenna positioned on top of the tractor. The stationary coordinates of the base station were surveyed at the time of first use and were used for all future runs of the same field. The imaging boom height was set at 135 cm from the camera lens to the ground, which resulted in a ground sample distance of 0.33 mm per pixel. The boom height was chosen to maximize resolution while ensuring the complete camera coverage of a single crop row per camera. The data collection operation was conducted within two hours of solar noon at a speed of approximately 1.9–2.1 km h<sup>-1</sup>, and the total run time to cover the TSWV field trial of one hectare was approximately one hour. The tractor traveled in a serpentine pattern by travelling down one pass and turning down the next pass in the opposite direction (Fig. 5). On completion, the camera SD cards were removed from the cameras, and the data was transferred to a separate computer using an SD card reader. The data with RTK-GPS points were transferred to the same computer via a network upload from the Raspberry Pi.

## 2.2. Geolocation of images to experimental plots

Individual experimental plot locations were recorded using the same RTK-GPS components. The rover system were removed from the tractor and placed on a monopole for handheld operation. A Raspberry Pi 3 with a touchscreen accessory was used to communicate with the RTK-GPS and log the plot ID of each experimental plot and the measured point. One hundred sample coordinates collected over 10 s were averaged and recorded by the Raspberry Pi. Using this device, a single plot location was recorded at the southeastern corner of each experimental plot. Each point was then extended by the known length and width of the experimental plots to determine the plot boundaries as uniform areas.

Individual images from both a6000 cameras were geolocated using the RTK-GPS system on the tractor by synchronizing the camera image timestamps with the RTK-GPS timestamps. This synchronization was achieved by calculating each camera's timestamp offset ( $t_{\text{offset}}$ ) from the RTK-GPS timestamp ( $t_{\text{gps1}}$ ) and camera timestamp ( $t_{\text{camera1}}$ ) that occurred in the same location using the formula (Eq. (1a))

$$t_{\text{offset}} = t_{\text{gps1}} - t_{\text{camera1}} \quad (1a)$$

Identifying the same location was conducted by visually identifying the first image that contains the start of the first plot in each left and right camera ( $t_{\text{camera1}}$ ), and the first RTK-GPS point timestamp ( $t_{\text{gps1}}$ ) with an associated point located within the first plot boundary was used. Every image was then assigned an RTK-GPS point that was associated

with the RTK-GPS point with the same timestamp ( $t_{\text{gpsX}}$ ) after the timestamp offset ( $t_{\text{offset}}$ ) was applied to the camera timestamp ( $t_{\text{cameraX}}$ ) using the formula (Eq. (1b))

$$t_{\text{gpsX}} = t_{\text{cameraX}} - t_{\text{offset}} \quad (1b)$$

Images with an RTK-GPS point within a plot boundary were distinctly associated since plot boundaries did not intersect.

## 2.3. Training the convolutional neural network

Images collected by the cameras were analyzed using a CNN trained on imagery collected from a TSWV peanut trial on July 10, 2018, 76 days after planting (DAP). Fourteen raw images were used as training data. One random training image was used from 12 selected plots where prior field notes showed a high level of disease presence. Two additional random images were also included from plots containing a TSWV resistant variety to include asymptomatic examples. Training images encompassed representative images of six different peanut varieties (FloRun 157, FloRun 331 (Tillman, 2019), Georgia-06G (Branch, 2007), Georgia 12Y (Branch, 2013), TUFRunner 297 (Tillman, 2018), and TUFRunner 511 (Tillman and Gorbet, 2017)). Raw images were split and converted into a total of 4704 unique 224 × 224 pixel JPEG training images using ImageMagick (7.0.8-20, [www.imagemagick.org](http://www.imagemagick.org)) and UFRaw (0.22, [ufraw.sourceforge.net](http://ufraw.sourceforge.net)) software programs.

Each 224 × 224 pixel image was individually labeled to be used for



**Fig. 1.** Examples of imagery (224x224 pixel) used to train the system to detect tomato spotted wilt virus (TSWV) symptoms (a) Stunting and mottling (b) Chlorosis, and (c) Asymptomatic peanut.

training. The labels used to classify the visual symptoms of TSWV were stunting and mottling, as well as chlorosis (Fig. 1). Asymptomatic peanut and ground labels were used to classify the remaining images. Ambiguous labels, or images containing multiple classes or rendered unidentifiable by the plant pathologist due to poor image quality, were omitted from the training set.

The training images were displayed at full scale, on a high definition computer monitor, and were arranged in their original locations to provide surrounding imagery. Two trained plant pathologists labeled the same imagery, and only image labels where both pathologists agreed were used for training. After excluding ambiguous labels and labels not in concurrence, 2,716 of the 4,704 unique training images remained.

The labeled training images were augmented by generating new images which varied in contrast and brightness by  $\pm 35\%$  and  $\pm 10\%$  respectively. Spatial variations were also generated using rotations of  $90^\circ$ ,  $180^\circ$ , and  $270^\circ$ , followed by a mirror flip on the vertical axis of each of the rotations. A total of 65,184 augmented images were used in training and validation (Table 1).

The CNN was trained using the transfer learning technique (Shin et al., 2016), reducing the training data and computation time required. An Inception v3 image classifier model (Fig. 2) (Szegedy et al., 2015) that was intensively trained on the iNaturalist image dataset (Van Horn et al., 2018) was used as the base network. The Inception v3 network was selected due to the unique availability of an iNaturalist trained variant. Using the TensorFlow Hub (Abadi et al., 2015, 2016) Python library, the base network was downloaded and trained on the labeled training images. The transfer learning technique replaces the final Softmax layer with new output classes and modifies only this layer's weights and biases during training. One percent of the training data, 652 images, was randomly removed from the training set and used to validate the model every seven iterations through the training set (epochs). Training executed with a constant learning rate of 0.02, and stopped once the validation set accuracy results plateaued at a 91% accuracy, after 756 epochs. Training was conducted on a single 1080ti GTX Graphical Processing Unit (NVIDIA, Santa Clara, CA, USA) and required 16 h of computation time.

#### 2.4. Cumulative confidence score

The system images were analyzed using the CNN model by evaluating 56x56 pixel sections of the image (Fig. 3). This was achieved by using a larger input-size CNN model and arranging the image input areas in an overlapping grid arrangement of four separate 224x224 pixel grids incrementally offset by 25% in both the abscissa and ordinate axes. Resulting in 56x56 pixel areas that were assessed by the CNN model a total of 16 times each with different surrounding imagery. Each CNN model assessment resulted in a continuous percentage confidence score of 0–1 for each of the four trained classes. Therefore, each 56x56 pixel area was the sum of each overlapping CNN model result, providing a 0–16 cumulative confidence score for each class.

#### 2.5. Confidence thresholding

Two plant pathologists labeled 56x56 pixel ground-truth images that were generated from five new tractor images of plots with high disease incidence occurring within a single pass of a TSWV peanut trial at a later

**Table 1**  
Number of 224x224 pixel images used in training and validation.

Class	Unique Images	Augmented Images
Stunting & mottling	227	5,448
Chlorosis	379	9,096
Ground	747	17,928
Asymptomatic	1,363	32,713
Total	2,716	65,184

date than the training images on August 14, 2018 (111 DAP). The same classes, including ambiguous labels, were used to classify the visual symptoms of TSWV, ground, and asymptomatic peanuts. After splitting the images, the initial imagery dataset was 20,650 images. Out of which 8,708 images were labeled as ambiguous by one or both of the pathologists and were removed. Nine hundred eighty seven additional images were removed due to being labeled differently. In total, 10,955 of the 20,650 images were used for the confidence thresholding analysis.

The same imagery was assessed by the CNN and was given a cumulative confidence score. Receiver Operator Characteristic (ROC) curves (Nettleman, 1988) were used to summarize the classification performance of the CNN models. A ROC curve is a plot of sensitivity as a function of  $(1 - \text{specificity})$  for the possible cut-offs (Agresti, 2007). The properties of a CNN model with a given confidence threshold or classification cut-off are determined by the probability of correctly classifying an image containing a feature of interest  $x$ , called sensitivity, and the probability of correctly classifying an image that does not contain feature  $x$ , called specificity. For a given specificity, better classification performance corresponds to higher sensitivity (Brownie et al., 1986). The better the classification performance of the model, the higher the ROC curve and the closer the area under the ROC curve is to a value of 1 (Agresti, 2007). A value of 0.50 means predictions were no better than random guessing for the classification. ROC curves were generated using the Python scikit-learn library (Pedregosa et al., 2011), where the confidence scores were compared against the labeled 56 × 56 pixel ground-truth dataset. The confidence threshold used for each of the four classes was the threshold that maximized the F1 Score. The F1 Score is the harmonic mean of precision and recall, and the F1 Score is widely used when one class is rare (Lipton, 2014), such as plant disease symptoms.

#### 2.6. Image analysis and CNN inference pipeline

Raw imagery and location data from the a6000 cameras and RTK-GPS system, along with the measured plot locations and dimensions, were used as the inputs for the image analysis and CNN inference pipeline (Fig. 4). The pipeline outputs the plot ID and the percentage coverage of each class at every 1.9 cm length interval.

Only imagery that was geolocated to a plot was analyzed. Images were converted into JPEG format and cropped using ImageMagick and UFRaw software programs. All images were cropped to a 3,304 pixel width, which completely included only one row in each image, with the two-camera system capturing the two center rows. To remove imagery overlap and double sampling in most areas, the image height was cropped at the bottom edge where the recorded RTK-GPS point did not exceed the vertical field of view of the prior image. The vertical field of view was calculated to 0.33 mm per pixel using the known camera and lens specifications and was constant due to a fixed camera height.

Each resulting image was analyzed by the CNN and produced a cumulative confidence score for each 56x56 pixel area. If the cumulative confidence score exceeded the confidence threshold for any given class, it was positively inferred that the area corresponded to any of those classes. A percentage coverage for each class was determined at every 56 pixel interval, or approximately every 1.8 cm, iterating vertically across each image. The percentage coverage was calculated by dividing the number of positively inferred by the total number of 56x56 pixel areas that were assessed across the width of the image. The inference pipeline provided multiple percentage coverages of TSWV symptoms (stunting and mottling, as well as chlorosis), ground, and asymptomatic peanut, each identified by plot ID.

#### 2.7. Tomato spotted wilt virus field trial

To evaluate the performance of the data collection, location, and image analysis pipeline, a TSWV peanut field experiment was implemented in 2019 consisting of 96 plots each measuring 9.2 m in length and 3.7 m in width (Fig. 5). The experiment was conducted at the North

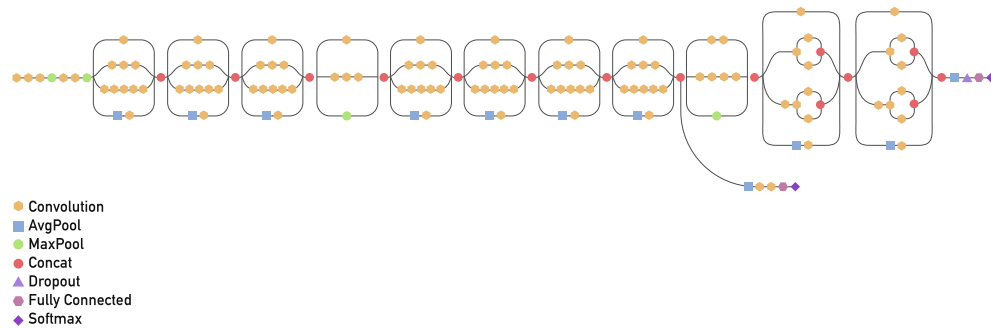


**Fig. 2.** Schematic diagram of the Inception v3 network architecture.



**Fig. 3.** Convolutional Neural Network (CNN) model “stunting and mottling” (red outline) results ( $56 \times 56$  pixel) on tractor imagery.

Florida Research and Education Center (NFREC), Quincy, FL ( $30^{\circ}32'N$ ,  $84^{\circ}35'E$ ). The experimental design for the field trial was a randomized complete block design consisting of three factors in a full factorial design. The three factors were peanut variety (FloRun 157, FloRun 331, Georgia-06G, Georgia-12Y, TUFRunner 297, and TUFRunner 511), application of Thimet in-furrow (yes or no), and two seeding rates (four or six seeds per 0.3 m of row). The six peanut varieties used in the experiment were selected for different levels of resistance to TSWV. These factors were selected to facilitate a range of severity levels. The standard visual method to assess the severity for field experiments involves rating every 0.3 m of peanut row for symptoms of TSWV for each plot and converting that number to a percentage of total row length (Patrick et al., 2017). In this experiment, the two center rows in each four-row plot were evaluated for incidence and severity of TSWV symptoms by a single pathologist from July 30, 2019 to August 1, 2019, nominally at 90 DAP. Severity was estimated as a percent severity of symptoms (stunting and mottling, as well as chlorosis) observed on foliage in each 0.3 m length of row. The tractor imaging system was operated on the same field on July 26, 2019 (85 DAP) and August 14, 2019 (104 DAP).

#### 2.8. Molecular TSWV testing

To test for the presence of TSWV, eighteen individual peanut plants were collected from the field experiment in 2019. Three plants were

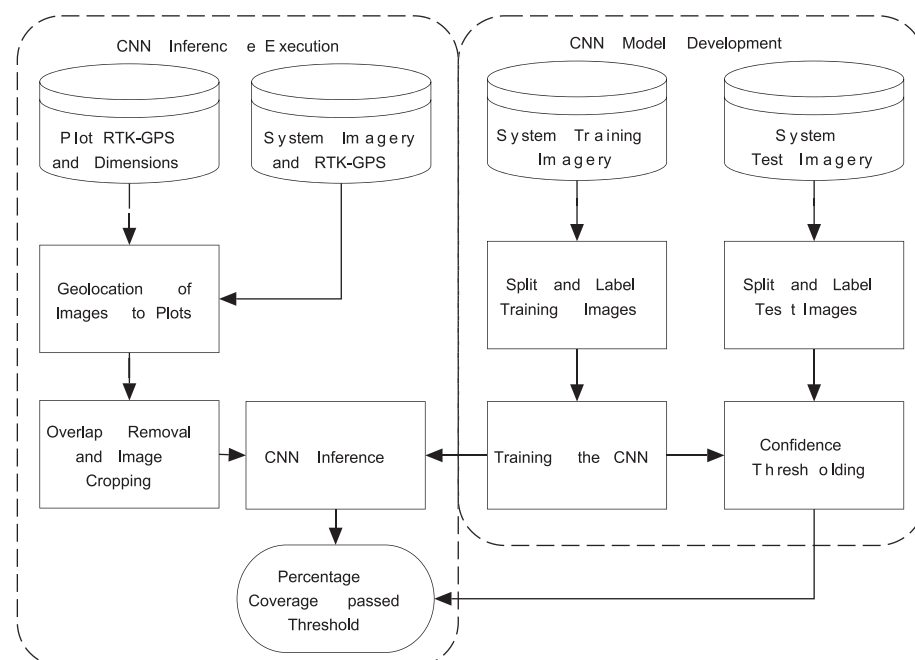


**Fig. 4.** CNN inference and model development pipelines.

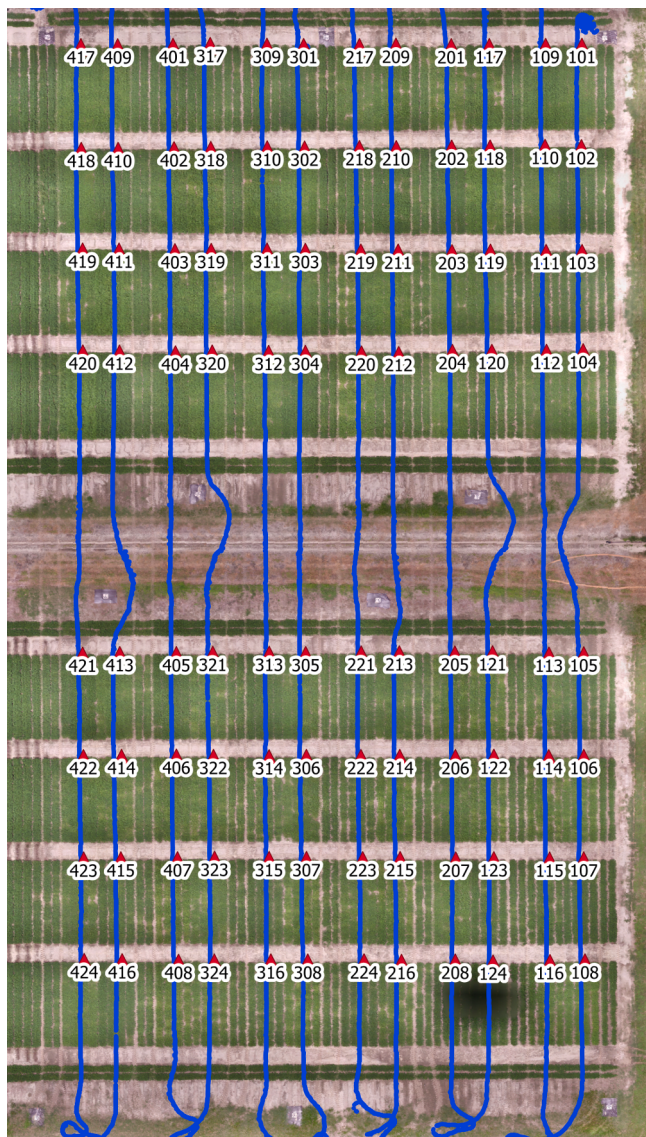


**Fig. 5.** Tomato spotted wilt field trial (orthoimage), plot IDs (black text), and position coordinates (blue line). Orthoimage collected on August 14, 2019 by aerial imaging system.

selected from each of the six varieties according to three selection phenotypes “stunting and mottling,” “non-stunted but chlorotic” and “asymptomatic”. For each plant, total RNA extracts (RNeasy Plant Mini Kit, Qiagen, Valencia, CA) from a mixture of peanut plant crowns and pegs were used as template for first strand cDNA synthesis using random hexamers and Moloney murine leukemia virus reverse transcriptase (Promega Corp., Madison, WI). Primers TSWV722 and TSWV723 that are specific for the nucleocapsid (N) protein gene of TSWV (Adkins and Rosskopf, 2002) and produce amplicons of 620 bp were used for polymerase chain reaction. Amplicons were analyzed by electrophoresis on 1% (w/v) agarose gels.

## 2.9. Statistical analysis

Data were statistically analyzed using JMP Pro version 15.0.0 (SAS Institute Inc., Cary, North Carolina, USA). To compare the visual assessment of TSWV symptom severity with the CNN-based assessments of chlorosis, or stunting and mottling, the plot level mean values were correlated using Pearson product-moment correlation.

To further compare visual vs automated assessment methods, we

analyzed the field experiment using the linear mixed models procedure with restricted maximum likelihood (REML) estimation of variance components. Two models were investigated: Model (1) using the natural log transformed visual percent severity rating as the response and Model (2) using natural log transformed CNN percent stunting and mottling as the response. For both models, variety, use of Thimet in-furrow, and seed spacing were considered fixed effects and block was considered a random effect. Effects were considered significant when  $P < 0.05$ . Least squares means (LS means) were compared using a Tukey’s honestly significant difference (HSD) post hoc test.

## 3. Results

### 3.1. ROC results

Initial CNN model performance results are provided by the ROC analysis conducted during confidence thresholding, where the CNN model results were evaluated against ground-truth assessments made in the same imagery by two plant pathologists. The resulting ROC curves for each of the four classes are shown (Fig. 6). The performance metrics used were the area under the receiver operating characteristic curve (AUC), F1 Score, sensitivity, and specificity (Table 2).

### 3.2. Plant sample testing for TSWV

Of the eighteen plant samples tested for TSWV by polymerase chain reaction, nine were positive (Table 3). For the plants selected as “stunted and mottled,” five of six plants tested positive for TSWV. For the plants selected as “non-stunted but chlorotic,” three of six tested positive for TSWV. For the plants selected as “asymptomatic,” one (a Georgia-06G plant) of six tested positive for TSWV.

### 3.3. Comparison between visual assessment and CNN-based assessment methods

The 96 plots that were assessed to compare the visual severity assessment with the CNN-based assessment ranged in plot level mean severity of TSWV symptoms from 0.24 to 14.9%, as determined by the trained plant pathologist. Significant positive correlations were observed among visual estimates of severity and the CNN-based assessments (Tables 4). A strong positive correlation was observed between visual assessment of severity of symptoms and CNN-based assessment of stunting and mottling ( $r = 0.78$ ,  $P < 0.0001$ ). A significant but weak to moderate correlation was observed between visual assessment of severity of symptoms and CNN-based assessment of chlorosis ( $r = 0.21$ ,  $P < 0.04$ ).

The TSWV field trial was analyzed using two linear mixed models. Model 1 utilized visually assessed severity as a response and Model 2 utilized CNN-based severity assessment as the response. No significant third order or second order interactions among fixed effects were detected with either model (Tables 5 and 6). Model outputs for both responses identified variety ( $P < 0.0001$ ) and use of Thimet in-furrow as significant main effects ( $P < 0.001$ ) (Tables 5 and 6).

Based on the post hoc analysis for the visual assessment of disease severity (Fig. 7), significantly lower levels of disease severity were observed with varieties Georgia-12Y, TUFRunner 297, and Georgia-06G relative to FloRun 331, TUFRunner 511 and FloRun 157 ( $P < 0.05$ ).

Similar results were observed using CNN-based assessment of “stunting and mottling” as a response (Fig. 8). Significantly lower levels of “stunting and mottling” were observed with varieties Georgia-12Y, TUFRunner 297, and Georgia-06G relative to FloRun 331, TUFRunner 511 and FloRun 157 ( $P < 0.05$ ).

## 4. Discussion

By combining two consumer-grade cameras with a low-cost RTK-GPS

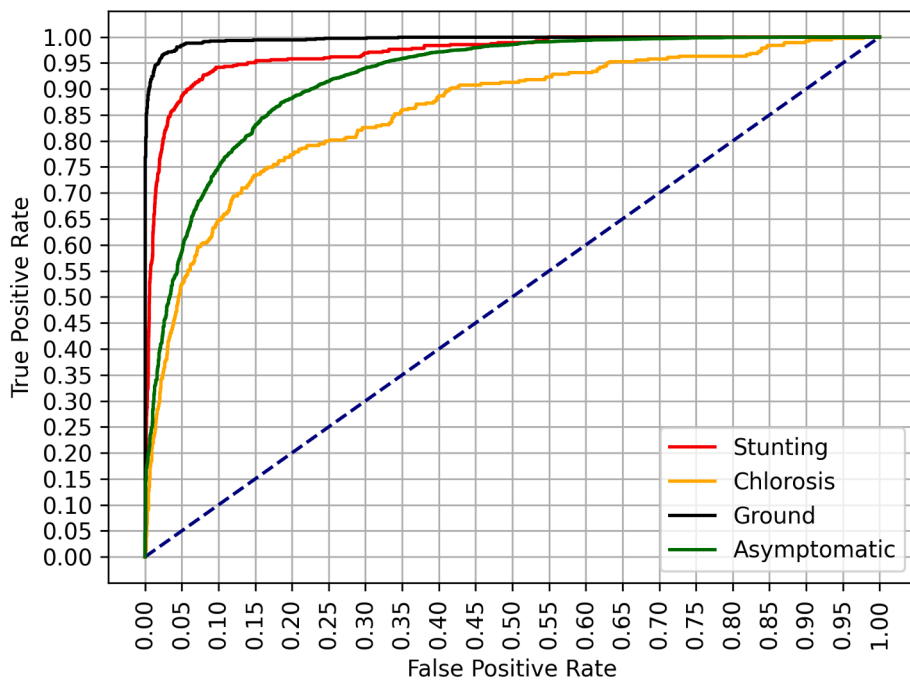


**Fig. 6.** Receiver Operator Characteristic (ROC) Curves of CNN model results (stunting, chlorosis, ground, asymptomatic) compared against pathologist verified imagery.

**Table 2**  
CNN performance on pathologist image labels.

Class	AUC	F1 Score	Sensitivity	Specificity
Stunting & mottling	0.969	0.714	0.765	0.980
Chlorosis	0.855	0.362	0.520	0.952
Ground	0.996	0.931	0.915	0.993
Asymptomatic	0.920	0.935	0.970	0.612

system and open-source CNN software we have created a high-throughput method to collect data under field settings, conduct image analysis, and to generate georeferenced plot level data. We were able to demonstrate that image analysis tools can be used effectively to assess disease severity under field conditions. To examine the effectiveness of the system, the CNN model results were compared with pathologist-classified imagery and with the results of the in-field-visual assessment method used to assess disease severity.

**Table 3**  
Plant samples tested for presence of TSWV.

Sample ID	Variety	Phenotype	Height (m)	Width (m)	No. of pods	Dry weight of pods (g)	PCR test result for TSWV
1	FLoRun 157	Asymptomatic	0.53	0.48	25	37.64	-
2	FLoRun 157	Non-stunted & chlorotic	0.30	0.65	48	49.74	-
3	FLoRun 157	Stunted	0.15	0.13	6	3.96	+
4	FloRun 331	Asymptomatic	0.37	0.37	35	31.62	-
5	FloRun 331	Non-stunted & chlorotic	0.33	0.91	85	83.47	+
6	FloRun 331	Stunted	0.26	0.62	20	18.78	+
7	Georgia-06G	Asymptomatic	0.22	0.49	21	27.98	+
8	Georgia-06G	Non-stunted & chlorotic	0.36	0.51	29	54.41	+
9	Georgia-06G	Stunted	0.17	0.26	1	0.2	+
10	Georgia-12Y	Asymptomatic	0.53	0.46	60	58.9	-
11	Georgia-12Y	Non-stunted & chlorotic	0.37	0.59	23	21.23	-
12	Georgia-12Y	Stunted	0.22	0.26	6	3.59	+
13	TufRunner 297	Asymptomatic	0.25	0.61	15	8.19	-
14	TufRunner 297	Non-stunted & chlorotic	0.38	0.91	45	58.88	+
15	TufRunner 297	Stunted	0.20	0.22	8	8.4	-
16	TufRunner 511	Asymptomatic	0.33	0.47	17	22.91	-
17	TufRunner 511	Non-stunted & chlorotic	0.45	0.30	29	39.05	-
18	TufRunner 511	Stunted	0.25	0.61	23	27.39	+

**Table 4**  
Parametric correlations among plot level means of visual estimates of TSWV symptom severity and plot level means of CNN-based assessments of symptoms.

	Visually assessed severity of symptoms		CNN percent "stunting and mottling"		CNN percent "chlorosis"	
	Pearson's correlation	Correlation prob.	Pearson's correlation	Correlation prob.	Pearson's correlation	Correlation prob.
Visually assessed severity of symptoms	1.00	-				
CNN percent "stunting and mottling"	0.78	<0.0001	1.00	-		
CNN percent "chlorosis"	0.21	0.04	0.36	<0.001	1.00	-

**Table 5**

Fixed effects tests for model 1 with natural log transformed visual assessment of TSWV symptom severity as response.

Source	DF	DF Den	F Ratio	Prob > F
Variety	5	69	14.16	<0.0001
Thimet in-furrow	1	69	58.20	<0.0001
Seed spacing	5	69	2.05	0.082
Variety * Thimet in-furrow	1	69	0.52	0.472
Variety * Seed spacing	5	69	0.26	0.933
Thimet in-furrow * Seed spacing	1	69	0.14	0.713
Variety * Thimet in-furrow * Seed spacing	5	69	0.64	0.673

**Table 6**

Fixed effects tests for model 2 with natural log transformed CNN-based assessment of stunting and mottling as response.

Source	DF	DF Den	F Ratio	Prob > F
Variety	5	69	11.41	<0.0001
Thimet in-furrow	1	69	24.87	<0.0001
Seed spacing	5	69	0.26	0.932
Variety * Thimet in-furrow	1	69	0.20	0.655
Variety * Seed spacing	5	69	0.32	0.898
Thimet in-furrow * Seed spacing	1	69	0.08	0.779
Variety * Thimet in-furrow * Seed spacing	5	69	0.27	0.928

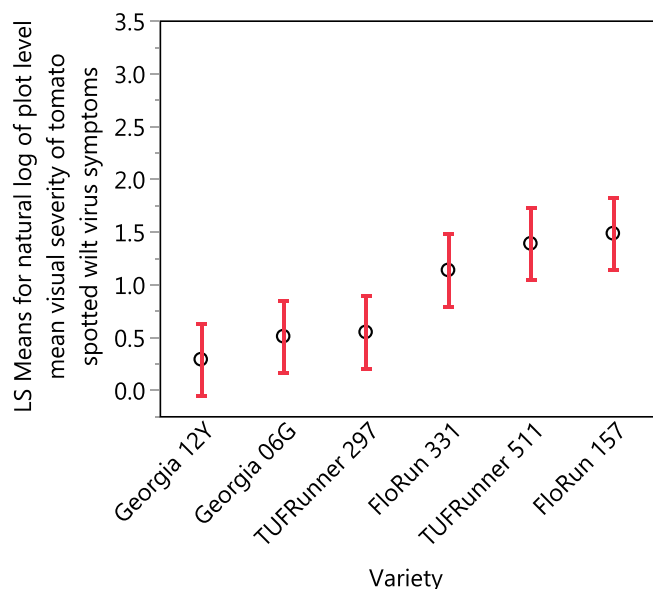


Fig. 7. Least squares means for natural log transformed plot level visual assessment of disease severity for six peanut varieties. Whiskers represent 95 percent confidence interval.

#### 4.1. CNN performance and ROC results

The test dataset comprised of imagery collected 35 days after the training data, which consisted of advanced crop maturity and disease infection. Under these conditions, the ROC for a critical label to detect symptoms of TSWV, "stunting and mottling," achieved a high AUC of 96.8%, whereas using the threshold that maximizes the F1 Score metric achieved a 98.0% specificity.

A poor F1 Score and sensitivity was observed for the "chlorosis" class. This classification challenge was due to leaf yellowing caused by factors other than or in addition to TSWV. This agrees with the mixed (50% agreement) results of the PCR-analysis of chlorotic peanut tissue. Differentiating TSWV-caused chlorosis from other causes was not possible using the system imagery. A common example of this occurrence was the light green color of new and rapidly growing leaf tissue.

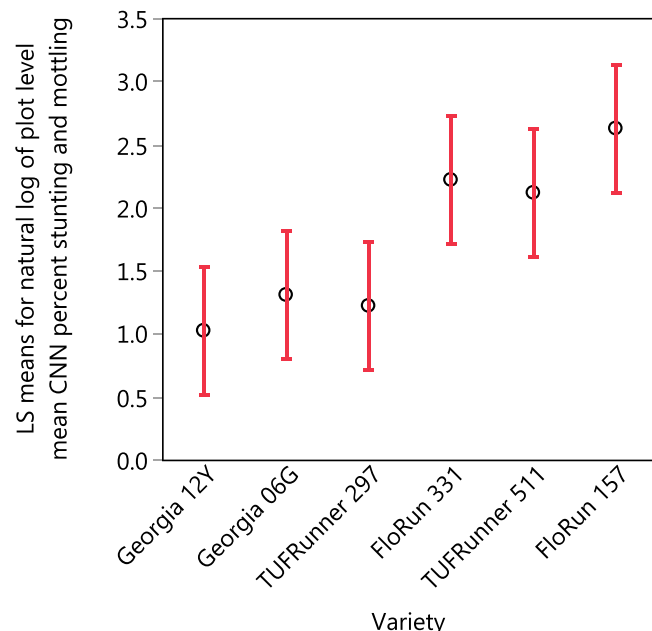


Fig. 8. Least squares means for natural log transformed plot level CNN-based assessment of "stunting and mottling" for six peanut varieties. Whiskers represent 95 percent confidence interval.

Furthermore, the use of a small training set and a constant learning rate may have overfitted the model to specific examples of chlorosis (Rawat and Wang, 2017). The accurate and consistent color reproduction in imagery with low-cost cameras in a field environment was challenging. Improving the "chlorosis" class may be possible with additional asymptomatic peanut training imagery, an improved model training protocol, and the use of color correction methods with higher quality cameras. A simple class to differentiate background from other classes of interest was "ground" which had an AUC of 99.6% and a 99.2% specificity. Due to the poorer results in "chlorosis," only the "stunting and mottling," "ground," and "asymptomatic" classes were used while comparing the system with the in-field rating methods.

The "asymptomatic" class was considered the single negative case of the classes. As such, the relatively poor specificity performance of this class can be explained by the incorrect classification of "chlorosis." Removing an output class from an existing CNN model is not possible, though a new model and thresholds can be created from new training and test data sets. Data on the areas occupied by the "asymptomatic" class is still informative as it provides a quantitative measure of the peanut canopy in each plot that did not show symptoms of stunting and mottling or chlorosis.

#### 4.2. Comparison between visual assessment and CNN-based method

The arrangement of CNN results provided a means to quantify areas containing features of interest (e.g. disease symptoms). Imagery from the ground-based platform was utilized to calculate high-resolution assessments (grid areas of under 2 cm classified for presence of visible symptoms), that provides a highly accurate estimate of the plot-level area of symptomatic peanut canopy. By contrast, the resolution of the visual assessment of disease was based on a fixed 30 cm interval.

In this study, the standard for comparison with the CNN-based system was visual assessment by a trained plant pathologist. Significant correlations were observed among the CNN-based models for specific symptoms and the visual assessment of disease severity. The CNN-based model for stunting and mottling demonstrated the strongest correlation with the visual assessment results. Visual estimates of disease severity are inherently subjective and may be influenced by the experience level

of the assessor as well as by challenging environmental conditions, such as heat and humidity (contributing to fatigue), which can result in inconsistent assessments over the duration of the assessment period (Bock et al., 2020). Given the known limitations associated with visual assessment, it is not surprising that the correlation between the visual assessment results and the CNN-based assessment was only moderately strong. However, the fact that the same main effects and differences among treatment levels were detected provides evidence that the CNN-based method was at least as effective as visual assessment. None of the varieties evaluated for this study were completely resistant to TSWV. However, there were significant differences among varieties in their level of disease severity, and their relative responses to TSWV were in line with results reported in previous studies (Patrick et al. 2017; Chappell et al. 2020). Post hoc analysis yielded the same separation of varieties for their mean severity whether using visual assessment or the CNN-based assessment of stunting and mottling. For example, Georgia-12Y, TUFRunner 297 and Georgia-06G demonstrated the lowest disease severity and differed significantly from varieties FloRun 331, TUFRunner 511 and FloRun 157.

Potential limitations of our CNN-based system include the fact that training data was classified by humans meaning that the model classification outputs will include any error/bias introduced by the humans that classified the training dataset. This issue was addressed by involving two trained plant pathologists during development of the training dataset and only using the data where the experts agreed about the presence of a symptom. Likewise, the model testing imagery was also confirmed by two pathologists, the results of which determined the confidence threshold used. Due to limitations with resolution of the a6000 imagery it was not possible to confidently classify other characteristic symptoms such as “ring spot”. With improved image resolution this might be possible and would likely improve the accuracy of the system.

Selected plants from each classification category were tested for the presence of TSWV to verify that symptoms were associated with presence of TSWV. Stunting and mottling was associated with presence of TSWV in 83% of cases, whereas chlorosis was associated with presence of the virus in only 50% of the plants tested. As noted earlier, the inconsistent detection of TSWV from chlorotic plants have been due to presence of chlorosis related to other common biotic or abiotic issues, such as nutrient deficiency. TSWV was only detected in one asymptomatic plant. Positive detection of TSWV from an asymptomatic plant may be due to an early stage infection (prior to symptom development) and/or a latent TSWV infection. It is important to note that detection of symptoms cannot be used in place of confirmation of pathogen presence but rather imagery-based systems (computer or human) are useful for comparisons of symptom development. As with human visual assessment, some error is expected since the same symptoms can have multiple causes and it is not practical or feasible to extensively test for presence of the virus in field trials.

#### 4.3. Future recommendations

Improving the quality of the imagery collected would improve the capability of the system to accurately classify a symptom feature as a disease-related symptom. Due to limitations with image resolution, certain characteristic features of TSWV were not feasible to detect (chlorotic ringspots). The Sony a6000 cameras and lenses used were a low-cost component relative to the entire system, while a professional full-frame camera with a fixed lens would provide a substantial improvement in image quality and symptom identification.

Further improvements in image classification accuracy would likely be gained from additional unique training imagery. The model training dataset consisted of 227 unique examples of stunting and mottling and 379 unique instances of chlorosis from a single time-period of data collection. By including multiple time periods of training data collection, it would provide additional variations in the lighting conditions,

crop maturities, and stages of disease progress which might improve model performance under those same real-world conditions.

This system utilizes a CNN classifier network effectively. However, other image analysis methods could be applied within the same system to produce novel results. As an example, an object detector CNN network such as Faster R-CNN (Ren et al., 2015) or YOLOv3 (Redmon and Farhadi, 2018) would provide a count of detected instances of disease symptoms, instead of the percent coverage result.

#### 4.4. System efficacy

This high-throughput CNN-based system alleviates the requirement for a trained plant pathologist or plant breeder to conduct field ratings. It would also ensure that disease assessments are consistent and reproducible across different locations over time.

A common limitation of utilizing a CNN for image analysis is the requirement of a large supervised training set. The collection and labelling of the imagery are a limitation due to the cost and effort involved. To overcome these limitations, the two methods known to effectively train a CNN on a smaller dataset were utilized; transfer learning and data augmentation (Yamashita et al., 2018). All image processing and machine learning software libraries used for the development of the system were open source, ensuring accessibility to these technologies and further reducing the cost of development. The sensing equipment used were widely available consumer cameras, a low-cost RTK-GPS geolocation system, and a Raspberry Pi microcomputer. The use of a tractor is optional, since the system can be applied to imagery collected using alternative means, such as a pushcart (Thompson et al., 2018; Crain et al., 2016).

The results of this study demonstrate the successful application of this tool for high-throughput disease severity assessment under field conditions and the potential utility of the system as a tool to quantify the response of peanut varieties to TSWV in an accurate, reproducible and efficient manner. This system has many potential applications within plant science. One immediate application will be for plant breeding purposes as a tool to conduct disease severity assessments and to assess other visible plant traits. Because the integrated RTK-GPS system collects accurate, georeferenced data in association with traits or features of interest, plant disease symptoms may be monitored over time and space. The ability to generate this type of data has the potential to enable rapid advances in fields such as plant disease epidemiology, crop improvement, and agronomy.

#### Funding

This research was funded by the University of Florida, IFAS.

#### CRediT authorship contribution statement

**James W. Clohessy:** Conceptualization, Methodology, Software, Validation, Formal analysis, Data curation, Writing - original draft, Writing - review & editing, Visualization, Supervision. **Santosh Sanjel:** Methodology, Data curation, Writing - original draft, Writing - review & editing. **G. Kelly O'Brien:** Resources, Data curation, Writing - original draft, Writing - review & editing. **Rebecca Barocco:** Methodology, Resources, Data curation, Writing - original draft, Writing - review & editing. **Shivendra Kumar:** Resources, Writing - review & editing. **Scott Adkins:** Methodology, Writing - review & editing. **Barry Tillman:** Resources, Writing - review & editing. **David L. Wright:** Writing - review & editing, Supervision, Project administration, Funding acquisition. **Ian M. Small:** Conceptualization, Methodology, Validation, Formal analysis, Writing - original draft, Writing - review & editing, Supervision, Project administration, Funding acquisition.

## Declaration of Competing Interest

The authors declare that they have no known competing financial interests or personal relationships that could have appeared to influence the work reported in this paper.

## Acknowledgments

Maynard Douglas, Chuck Dickson, Derek Hurley, Ethan Bolton and other members of the AgPath crew, Shannon Darby, Chad Parramore, Russell Hunter and other members of the NFREC Staff, UF IFAS IT, UF Research Computing, Carrie Vanderspool of USDA-ARS.

## References

- Abadi, M., Agarwal, A., Barham, P., Brevdo, E., Chen, Z., Citro, C., Corrado, G.S., Davis, A., Dean, J., Devin, M., Ghemawat, S., Goodfellow, I., Harp, A., Irving, G., Isard, M., Jia, Y., Jozefowicz, R., Kaiser, L., Kudlur, M., Levenberg, J., Mane, D., Monga, R., Moore, S., Murray, D., Olah, C., Schuster, M., Shlens, J., Steiner, B., Sutskever, I., Talwar, K., Tucker, P., Vanhoucke, V., Vasudevan, V., Viegas, F., Vinyals, O., Warden, P., Wattenberg, M., Wicke, M., Yu, Y., Zheng, X., 2015. TensorFlow: Large-scale machine learning on heterogeneous distributed systems 19.
- Abadi, M., Barham, P., Chen, J., Chen, Z., Davis, A., Dean, J., Devin, M., Ghemawat, S., Irving, G., Isard, M., Kudlur, M., Levenberg, J., Monga, R., Moore, S., Murray, D.G., Steiner, B., Tucker, P., Vasudevan, V., Warden, P., Wicke, M., Yu, Y., Zheng, X., 2016. TensorFlow: A system for large-scale machine learning 21.
- Adkins, S., Rosskopf, E.N., 2002. Key West Nightshade, a new experimental host for plant viruses. *Plant Dis.* 86, 1310–1314. <https://doi.org/10.1094/PDIS.2002.86.12.1310>.
- Agresti, A., 2007. *An Introduction to Categorical Data Analysis*, second ed. Wiley-Interscience, Hoboken, NJ.
- Albawi, S., Mohammed, T.A., Al-Zawi, S., 2017. Understanding of a convolutional neural network. 2017 International Conference on Engineering and Technology (ICET), pp. 1–6. doi: 10.1109/ICEngTechnol.2017.8308186.
- Anco, D.J., Thomas, J.S., Monfort, W.S., 2019. Efficacy and profitability of insecticide treatments for tomato spotted wilt management on peanut in South Carolina. *Plant Dis.* 104, 1096–1104. <https://doi.org/10.1094/PDIS-09-19-1829-RE>.
- Branch, W.D., 2007. Registration of 'Georgia-06G' peanut. *J. Plant Reg.* 1, 120.
- Branch, W.D., 2013. Registration of 'Georgia-12Y' peanut. *J. Plant Reg.* 7, 151–153.
- Bock, C.H., Barbedo, J.G.A., Del Ponte, E.M., Bohnenkamp, D., Mahlein, A.-K., 2020. From visual estimates to fully automated sensor-based measurements of plant disease severity: status and challenges for improving accuracy. *Phytopathol. Res.* 2, 9. <https://doi.org/10.1186/s42483-020-00049-8>.
- Brownie, C., Habicht, J.P., Cogill, B., 1986. Comparing indicators of health or nutritional status. *Am. J. Epidemiol.* 124 (6), 1031–1044. <https://doi.org/10.1093/oxfordjournals.aje.a114473>.
- Chappell, T.M., Codod, C.B., Williams, B.W., Kemeraite, R.C., Culbreath, A.K., Kennedy, G.G., 2020. Adding epidemiologically important meteorological data to peanut Rx, the risk assessment framework for spotted wilt of peanut. *Phytopathology* 110, 1199–1207. <https://doi.org/10.1094/PHYTO-11-19-0438-R>.
- Crain, J.L., Wei, Y., Barker, J., Thompson, S.M., Alderman, P.D., Reynolds, M., Zhang, N., Poland, J., 2016. Development and deployment of a portable field phenotyping platform. *Crop Sci.* 56, 965–975. <https://doi.org/10.2135/cropsci2015.05.0290>.
- Culbreath, A.K., Todd, J.W., Brown, S.L., 2003. Epidemiology and management of tomato spotted wilt in peanut. *Annu. Rev. Phytopathol.* 41, 53–75. <https://doi.org/10.1146/annurev.phyto.41.052002.095522>.
- Culbreath, A.K., Srinivasan, R., 2011. Epidemiology of spotted wilt disease of peanut caused by Tomato spotted wilt virus in the southeastern U.S. *Virus Research. Plant Virus. Virus Vect.: Exploit. Agric. Natural Ecosyst.* 159, 101–109. <https://doi.org/10.1016/j.virusres.2011.04.014>.
- DeChant, C., Wiesner-Hanks, T., Chen, S., Stewart, E.L., Yosinski, J., Gore, M.A., Nelson, R.J., Lipson, H., 2017. Automated identification of northern leaf blight-infected maize plants from field imagery using deep learning. *Phytopathology* 107, 1426–1432. <https://doi.org/10.1094/PHYTO-11-16-0417-R>.
- Deckert, C., Bolstad, P.V., 1996. Forest canopy, terrain, and distance effects on global positioning system point accuracy 5.
- FAOSTAT [WWW Document], n.d. URL <http://www.fao.org/faostat/en/#data/QC> (accessed 4.22.20).
- Fuentes, A., Yoon, S., Kim, S.C., Park, D.S., 2017. A robust deep-learning-based detector for real-time tomato plant diseases and pests recognition. *Sensors* 17, 2022. <https://doi.org/10.3390/s17092022>.
- Jackson, J., Davis, B., Gebre-Egziabher, D., 2018. A performance assessment of low-cost RTK GNSS receivers, in: 2018 IEEE/ION Position, Location and Navigation Symposium (PLANS). Presented at the 2018 IEEE/ION Position, Location and Navigation Symposium (PLANS), pp. 642–649. <https://doi.org/10.1109/PLANS.2018.8373438>.
- Kc, K., Yin, Z., Wu, M., Wu, Z., 2019. Depthwise separable convolution architectures for plant disease classification. *Comput. Electron. Agric.* 165, 104948. <https://doi.org/10.1016/j.compag.2019.104948>.
- Krizhevsky, A., Sutskever, I., Hinton, G.E., 2012. ImageNet classification with deep convolutional neural networks. In: Pereira, F., Burges, C.J.C., Bottou, L., Weinberger, K.Q. (Eds.), *Advances in Neural Information Processing Systems 25*. Curran Associates Inc, pp. 1097–1105.
- Lee, L., Jones, M., Ridenour, G.S., Bennett, S.J., Majors, A.C., Melito, B.L., Wilson, M.J., 2016. Comparison of accuracy and precision of GPS-enabled mobile devices. In: 2016 IEEE International Conference on Computer and Information Technology (CIT). IEEE, pp. 73–82.
- Lipton, 2014. Thresholding Classifiers to Maximize F1 Score [WWW Document]. DeepAI. URL <https://deepai.org/publication/thresholding-classifiers-to-maximize-f1-score> (accessed 8.27.20).
- Liu, B., Zhang, Y., He, D., Li, Y., 2018. Identification of apple leaf diseases based on deep convolutional neural networks. *Symmetry* 10, 11. <https://doi.org/10.3390/sym10010011>.
- Ma, J., Du, K., Zheng, F., Zhang, L., Gong, Z., Sun, Z., 2018. A recognition method for cucumber diseases using leaf symptom images based on deep convolutional neural network. *Comput. Electron. Agric.* 154, 18–24. <https://doi.org/10.1016/j.compag.2018.08.048>.
- Madden, L.V., Hughes, C., van den Bosch, F., 2017. *The Study of Plant Disease Epidemics, Epidemiology*. The American Phytopathological Society (APS Press), pp. Xiv-421. <https://doi.org/10.1094/9780890545058.fm>.
- Mahlein, A.-K., 2016. Plant disease detection by imaging sensors—parallels and specific demands for precision agriculture and plant phenotyping. *Plant Dis.* 100, 241–251.
- Mohanty, S.P., Hughes, D.P., Salathé, M., 2016. Using deep learning for image-based plant disease detection. *Front. Plant Sci.* 7 <https://doi.org/10.3389/fpls.2016.01419>.
- Naidu, R.A., Kimmims, F.M., Deom, C.M., Subrahmanyam, P., Chiyembekeza, A.J., van der Merwe, P.J.A., 1999. Groundnut Rossette: A virus disease affecting groundnut production in sub-Saharan Africa. *Plant Dis.* 83, 700–709. <https://doi.org/10.1094/PDIS.1999.83.8.700>.
- Nettleman, M.D., 1988. Receiver Operator Characteristic (ROC) curves. *Infect. Control Hosp. Epidemiol.* 9, 374–377. <https://doi.org/10.2307/30145466>.
- Nilsson, H., 1995. *Remote sensing and image analysis in plant pathology*. *Annu. Rev. Phytopathol.* 33 (1), 489–528.
- Patrick, A., Pelham, S., Culbreath, A., Holbrook, C.C., De Godoy, I.J., Li, C., 2017. High throughput phenotyping of tomato spot wilt disease in peanuts using unmanned aerial systems and multispectral imaging. *IEEE Instrum. Meas. Mag.* 20, 4–12. <https://doi.org/10.1109/MIM.2017.7951684>.
- Pedregosa, F., Varoquaux, G., Gramfort, A., Michel, V., Thirion, B., Grisel, O., Blondel, M., Prettenhofer, P., Weiss, R., Dubourg, V., Vanderplas, J., Passos, A., Cournapeau, D., Brucher, M., Perrot, M., Duchesnay, É., 2011. Scikit-learn: Machine learning in Python. *J. Mach. Learn. Res.* 12, 2825–2830.
- Ramcharan, A., Baranowski, K., McCloskey, P., Ahmed, B., Legg, J., Hughes, D.P., 2017. Deep learning for image-based cassava disease detection. *Front. Plant Sci.* 8 <https://doi.org/10.3389/fpls.2017.01852>.
- Rawat, W., Wang, Z., 2017. Deep convolutional neural networks for image classification: a comprehensive review. *Neural Comput.* 29, 2352–2449. [https://doi.org/10.1162/neco\\_a\\_00990](https://doi.org/10.1162/neco_a_00990).
- Redmon, J., Farhadi, A., 2018. Yolov3: An incremental improvement. arXiv preprint arXiv:1804.02767.
- Ren, S., He, K., Girshick, R., Sun, J., 2015. Faster r-cnn: Towards real-time object detection with region proposal networks. arXiv preprint arXiv:1506.01497.
- Rumelhart, D.E., 1986. Parallel distributed processing: Explorations in the microstructure of cognition. Learning internal representations by error propagation 1, 318–362.
- Savary, S., Willocquet, L., Pethybridge, S.J., Esker, P., McRoberts, N., Nelson, A., 2019. The global burden of pathogens and pests on major food crops. *Nature Ecol. Evol.* 3, 430–439. <https://doi.org/10.1038/s41598-018-0793-y>.
- Shin, H.-C., Roth, H.R., Gao, M., Lu, L., Xu, Z., Nogues, I., Yao, J., Mollura, D., Summers, R.M., 2016. Deep convolutional neural networks for computer-aided detection: CNN architectures, dataset characteristics and transfer learning. *IEEE Trans. Med. Imaging* 35, 1285–1298. <https://doi.org/10.1109/TMI.2016.2528162>.
- Sladojevic, S., Arsenovic, M., Anderla, A., Culibrk, D., Stefanovic, D., 2016. Deep neural networks based recognition of plant diseases by leaf image classification [WWW Document]. *Comput. Intell. Neurosci.* <https://doi.org/10.1155/2016/3289801>.
- Strange, R.N., Scott, P.R., 2005. Plant disease: A threat to global food security. *Annu. Rev. Phytopathol.* 43, 83–116. <https://doi.org/10.1146/annurev.phyto.43.113004.133839>.
- Szegedy, C., Liu, W., Jia, Y., Sermanet, P., Reed, S., Anguelov, D., Erhan, D., Vanhoucke, V., Rabinovich, A., 2015. Going deeper with convolutions. In: Presented at the Proceedings of the IEEE Conference on Computer Vision and Pattern Recognition, pp. 1–9.
- Tillman, B.L., Gorbet, D.W., 2017. Registration of 'TUFRunner '511'' Peanut. *J. Plant Reg.* 11, 235–239. <https://doi.org/10.3198/jpr2016.11.0064crc>.
- Tillman, Barry L., 2018. Registration of 'TUFRunner '297'' Peanut. *J. Plant Reg.* 12, 31–35. <https://doi.org/10.3198/jpr2017.02.0007cr>.
- Tillman, Barry L., 2019. FloRun™ '331' Peanut Variety. SS-AGR-425. University of Florida Institute of Food and Agricultural Sciences, Gainesville. <https://edis.ifas.ufl.edu/pdffiles/AG/AG4250.pdf> (accessed September, 14, 2020).
- Thompson, A.L., Thorp, K.R., Conley, M., Andrade-Sanchez, P., Heun, J.T., Dyer, J.M., White, J.W., 2018. Deploying a proximal sensing cart to identify drought-adaptive traits in upland cotton for high-throughput phenotyping. *Front. Plant Sci.* 9 <https://doi.org/10.3389/fpls.2018.00507>.

- Van Horn, G., Mac Aodha, O., Song, Y., Cui, Y., Sun, C., Shepard, A., Adam, H., Perona, P., Belongie, S., 2018. The iNaturalist Species Classification and Detection Dataset. arXiv: 1707.06642 [cs].
- Yamashita, R., Nishio, M., Do, R.K.G., Togashi, K., 2018. Convolutional neural networks: an overview and application in radiology. *Insights Imaging* 9, 611–629. <https://doi.org/10.1007/s13244-018-0639-9>.
- Zhang, X., Qiao, Y., Meng, F., Fan, C., Zhang, M., 2018. Identification of maize leaf diseases using improved deep convolutional neural networks. *IEEE Access* 6, 30370–30377. <https://doi.org/10.1109/ACCESS.2018.2844405>.